RHEED and STM studies of the pseudo-tenfold surface of the ξ'-Al$_{77.5}$Pd$_{19}$Mn$_{3.5}$ approximant crystal

H. R. Sharma,[1,2,*] M. Shimoda,[1,2] V. Fournée,[3] A. R. Ross,[4] T. A. Lograsso,[4] and A. P. Tsai[1,2,5]

[1]*National Institute for Materials Science, 1-2-1 Sengen, Tsukuba, Ibaraki, 305-0047, Japan*
[2]*SORST, Japan Science and Technology Agency, Japan*
[3]*LSG2M, CNRS-UMR7584, Ecole des Mines, Parc de Saurupt, 54042 Nancy, France*
[4]*Department of Materials Science and Engineering, Ames Laboratory, Ames, Iowa 50011, USA*
[5]*Institute of Multidisciplinary Research for Advanced Materials, Tohoku University, Sendai, 980-8577, Japan*

The pseudo-tenfold surface of the ξ'-Al$_{77.5}$Pd$_{19}$Mn$_{3.5}$ crystal, an approximant of the icosahedral Al–Pd–Mn quasicrystal, is investigated by reflection high-energy electron diffraction (RHEED) and scanning tunneling microscopy. The observed RHEED patterns of the surface after sputtering are found to be consistent with those of a simple cubic lattice with $(1\bar{1}0)$ surface plane. The [001] and [110] axes of the surface plane are oriented along the principal low-index axes of the bulk. The RHEED patterns of the sputter-annealed surface consist of diffraction streaks with periodic spacings expected for the bulk truncated surface. The surface prepared under different preparation methods is found to exhibit different step-height distribution and terrace morphology. A longer annealing yields a high density of shallow pentagonal pits on terraces, separated predominantly by 0.80-nm high steps and occasionally by double steps. In contrast, the surface prepared with shorter annealing time exhibits highly perfect terraces with 0.80-nm-high steps and additional unusual steps of heights close to 0.40 nm. All step heights observed for both preparation methods are consistent with interlayer spacings of the bulk model.

I. INTRODUCTION

Quasicrystals are a new class of solid materials often possessing conventionally forbidden rotational symmetries such as fivefold or tenfold. The existence of long-range order without periodicity is the most striking feature of quasicrystals. They are intermetallic compounds normally found in a narrow chemical composition range of the phase diagram.[1] For compositions close to that of the quasicrystals, one usually finds crystalline phases of various types. Among them are approximants, which have large unit cells and a local structure similar to that of the respective quasicrystals.[2] Many of their chemical and physical properties are also similar.[3] Due to their intimate relationship with quasicrystals, approximants are used in modeling the complex structure of quasicrystalline phases.[2]

Aside from their intriguing structure, quasicrystals exhibit very interesting surface properties such as a low surface energy and a low coefficient of friction.[4] Because of these fascinating surface features as well as potential applications related to surface phenomena,[4] special attention is given to quasicrystal surface studies. So far, the preparation and characterization of high-symmetry surfaces of icosahedral (i) Al–Pd–Mn,[5–19] i-Al–Cu–Fe,[20–26] and decagonal (d) Al–Ni–Co[20,27–38] quasicrystals have been widely investigated by various surface sensitive techniques: namely, by low-energy electron diffraction,[6–8,21,22,27,30,36,38] scanning tunneling microscopy,[5,10,11,17,18,20,24,26,28,32,33,36–38] He atom scattering,[17,34,35,38] Auger electron spectroscopy,[21,29,37] x-ray photoelectron spectroscopy,[25] and x-ray photoelectron diffraction.[12–15,19,31] Some of these studies have shown that different surface terminations are possible under different

treatments, specifically sputtering and annealing. Upon sputtering, light atoms are preferentially removed and the surface transforms into crystalline phases.[8,12–14,16,22,25,29] Annealing the sputtered surface at appropriate temperature recovers the quasicrystalline symmetry, which can usually be explained in terms of the respective bulk models. The surface prepared by sputter annealing usually yields a step-terrace structure and the step-terrace morphology is found to be dependent on various parameters during surface preparation.[18,33] It has been further shown that a more or less similar cleaning process employed on samples extracted from different ingots may yield nonidentical step-height distributions. For example, scanning tunneling microscopy of the fivefold surface of i-Al–Pd–Mn reported by Schaub *et al.* shows two different step heights,[5] while the same surface investigated by Shen *et al.* and Barbier *et al.* exhibits an additional step height.[10,17] The thermal history during the sample growth process as well as the subsequent annealing treatments can influence the surface morphology.[39]

In contrast to this comprehensive information available on quasicrystal surfaces, knowledge regarding the surface phenomena of approximant phases is much more limited. It would be interesting to learn whether or not similar surface phenomena as observed in quasicrystals are equally possible in these phases. For this, we have investigated the pseudo-tenfold surface of the ξ'-Al$_{77.5}$Pd$_{19}$Mn$_{3.5}$ crystal, an approximant of one of the intensively studied quasicrystals, i-Al–Pd–Mn, by employing reflection high-energy electron diffraction (RHEED) and scanning tunneling microscopy (STM). We have examined structural transitions in the surface region induced by sputter annealing as well as the morphology of the surface prepared under different conditions.

The bulk structure of the ξ'-Al–Pd–Mn phase can be described by an orthorhombic crystal with lattice constants $a_{\xi'} = 2.389$ nm, $b_{\xi'} = 1.656$ nm, and $c_{\xi'} = 1.256$ nm.[40] Along the $b_{\xi'}$ axis (which is equivalent to the pseudo-tenfold axis), four different types of layers are stacked at $y = 0$, 0.12, 0.16, and 0.25 in units of $b_{\xi'}$. The rest of the layers in the unit cell can be obtained by symmetry operations. Earlier reports on STM studies of the pseudo-tenfold surface of this approximant suggest that the surface terminates at specific pairs of layers.[41,42] However, with the present preparation conditions we additionally found that the pair can break into smaller sets of planes occasionally.

II. EXPERIMENT

The single-grain ξ'-Al$_{77.5}$Pd$_{19}$Mn$_{3.5}$ approximant grown by the Bridgman method was cut perpendicular to the pseudo-tenfold axis and then mechanically polished down to 0.25 μm using diamond paste. The sample was mounted on a molybdenum holder and inserted into the preparation chamber (base pressure 1×10^{-10} mbar) which is equipped with RHEED, an ion gun, and a sample heating mechanism. The surface was prepared by repeated cycles of sputtering (Ar$^+$, 2–3 keV, 15–30 min) and annealing (up to 580 °C). The temperature was measured by an optical pyrometer assuming that the emissivity of the surface is similar to that of the i-Al–Pd–Mn ($\epsilon = 0.36$). Changes in surface structure during the cleaning process were monitored by RHEED with an incident electron beam of 30 keV. The chemical composition of the sputtered and annealed surface was determined by x-ray photoemission spectroscopy (XPS). XPS measurements were performed using a VG ESCALAB MkII spectrometer and Mg $K\alpha$ radiation (1254 eV).

After preparation, the sample was transferred into the STM chamber and images were recorded using an Omicron room-temperature STM with a PtIr tip. The tunneling current and bias voltage used in the measurements were 0.14–0.30 nA and 1.3–2.5 V, respectively.

The chambers used for surface preparation and XPS and STM measurements are connected with each other so that the sample can be transferred among them without exposing it to the air.

III. RESULTS AND DISCUSSION

A. Reflection high-energy electron diffraction

1. Sputtered surface

RHEED patterns recorded from the sputtered surface are shown in Figs. 1(a)–1(f). These patterns were obtained at different angles of rotation of the sample around the surface normal—i.e., the $\mathbf{b}_{\xi'}$ axis. As seen, all observed patterns consist of spots aligned in straight lines. These kinds of patterns are normally formed by diffraction of electrons transmitted through crystalline islands present on the surface. The observed RHEED patterns hence suggest significant roughness, as expected for a sputtered surface. Therefore, we did not attempt to measure STM on this rough surface. It is practically hopeless to achieve meaningful STM images on such a
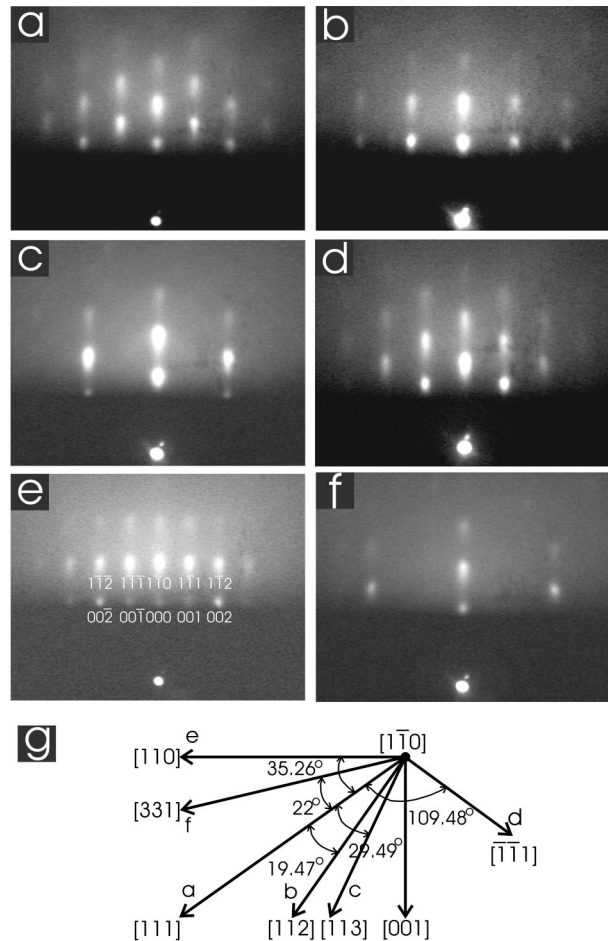

FIG. 1. RHEED patterns (a)–(f) of the sputtered pseudo-tenfold surface of the ξ'-Al$_{77.5}$Pd$_{19}$Mn$_{3.5}$ approximant recorded at different angles of rotation around the surface normal. The rotation angles are close to the angles between different axes of a cubic lattice (g) (the angles given are the exact angles between the axes; measurement angles are given in text). Indexing of the pattern for [110] incidence is given.

rough surface. The triangular and rectangular patterns shown in Figs. 1(a) and 1(e) are observed at a rotation of 35°, which is close to the angle between the [111] and [110] axes of a cubic lattice. These patterns can indeed be explained by the diffraction from a cubic lattice with an $(1\bar{1}0)$-type surface plane for the incident beam along the [111] and [110] axes, respectively. Similarly, diffraction patterns presented in Figs. 1(b)–1(d) appear at 20°, 33°, and 114° rotation from the position of the triangular pattern (anticlockwise rotation in the given figure), while the pattern given in Fig. 1(f) is measured at 20° rotation (clockwise) from the same position. The observed rotation angles are very close to the angles of the [112], [113], [$\bar{1}\bar{1}1$], and [331] axes from the [111] axis of a cubic lattice as shown in Fig. 1(g). As the triangular and rectangular patterns, these diffraction patterns are also found to be consistent with diffraction from the same cubic lattice with the $(1\bar{1}0)$-type surface plane for the incident beam along the [112], [113], [$\bar{1}\bar{1}1$], and [331] axes. The indexing of the RHEED pattern for [110] incidence is illustrated in

Fig. 1(e), which reveals that no extinction of diffraction spots happens unlike in diffraction patterns of bcc or fcc lattices. The observed RHEED patterns are hence consistent with those of a simple cubic lattice.

The chemical composition of the surface determined by measuring the intensity of Al $2p$, Pd $3d$, and Mn $3d_{3/2}$ core-level photoemission is found to be $Al_{63}Pd_{35}Mn_2$. The obtained composition shows a depletion of Al in the surface region, which is due to the preferential sputtering of this lighter element.[4,22] It is known that the phase diagram of Al–Pd–Mn contains CsCl-type Al–Pd phases on the Al-poor side.[43] Sputtering thus shifts the surface composition towards that of these CsCl-type phases. The lattice constant of the cubic structure estimated from the observed RHEED patterns is about 0.30 nm, which is indeed close to that of CsCl-type Al–Pd (0.304 nm).[44] These results suggest that the obtained RHEED patterns result from the structure related to the CsCl-type Al–Pd phase.

Various experimental techniques have shown that sputtering of quasicrystal surfaces can induce a crystalline layer (hereafter sputter-induced layer) in the surface region.[8,12–14,16,22,25,29] Shi *et al.* performed a structural characterization by dynamical low-energy electron diffraction (LEED) of the crystalline overlayer obtained by sputtering and annealing at 377 °C the surface of the *i*-Al–Cu–Fe quasicrystal.[22] This study revealed a CsCl-type structure with Al atoms at the corner sites and transition metal atoms (Cu, Fe) atoms randomly distributed at the body-center sites. A recent RHEED study of the same system by Barrow *et al.* showed that diffraction patterns of the surface directly after sputtering exhibit the bcc extinction rule.[25] This can only be explained if Al and transition metal atoms (Cu, Fe) randomly occupy the corner and body-center sites of the CsCl-type lattice. Thus the chemical ordering among the corner and body-center atoms deduced from dynamical LEED experiments must appear during the low-temperature annealing mentioned above. In the present case of the sputtered pseudo-tenfold surface, however, no such extinction of diffraction spots is observed directly after sputtering, implying that the sputter-induced layer maintains a chemical ordering among the species on the corner sites and body-center sites.

It is not clear why chemical disordering is observed on the quasicrystal surface and not on the approximant. It may be due to the different substrates or simply due to different sputtering conditions (at 5-keV Ar^+ beam was used in Barrow *et al.*[25] compared to the 2–3 keV Ar^+ beam used in the present case). Ions of lower energy may be less efficient in producing sufficient chemical disorder to achieve complete randomness of the chemical species occupying the two types of CsCl-type lattice sites necessary to observe the bcc extinction rule.

Furthermore, the sputtered quasicrystal surfaces normally contain n domains oriented along the degenerate n-fold high-symmetry directions of the quasicrystalline substrate, with $n=5$ and 10 for the fivefold and tenfold surfaces, respectively (hereafter multiply twinned domains).[12–14,45,16,25,45] A characteristic feature of RHEED patterns of, for example, the tenfold *d*-Al–Ni–Co surface is that equivalent patterns are observed at every 36° rotation around the tenfold axis.[45] In addition, diffraction patterns for the incident beam along the
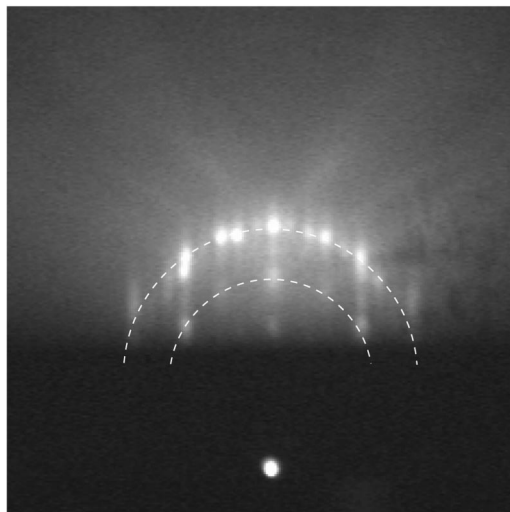

FIG. 2. RHEED pattern of the sputter-annealed pseudo-tenfold surface of the ξ'-$Al_{77.5}Pd_{19}Mn_{3.5}$ approximant (annealing temperature 550 °C). The incident beam direction is the same as for the pattern shown in Fig. 1(e).

[111] and [110] axes overlap[45] because the angle between the [111] and [110] axes is very close to 36°. RHEED patterns of the present surface do not show such overlapping, suggesting the absence of a multiply twinned domain structure, which is a noticeable difference with respect to the structure of the sputtered quasicrystal surfaces.

2. Annealed surface

RHEED patterns were recorded during annealing of the sputtered surface. At temperatures around 350 °C, diffraction spots begin to become faint and vertical streaks start to appear (not shown). An example of a RHEED pattern after annealing at 550 °C is shown in Fig. 2. This pattern was measured with the incident beam along the same direction as that of the pattern presented in Fig. 1(e)—i.e., the [110] axis of the simple cubic lattice associated with the sputter-induced layer. As seen, the original spotty pattern is replaced by a streaked pattern with brighter spots on circles, which is a typical feature of RHEED patterns from an appreciably smooth surface. This pattern consists of weak and strong streaks that yield a periodic spacing. The lattice parameter estimated from the distance between the nearest streaks is about 1.2 nm, which is close to the bulk lattice constant $c_{\xi'} = 1.256$ nm. The incident beam direction of this pattern is hence identified as parallel to the $a_{\xi'}$ axis. This reveals that the sputter-induced layer is formed with the [110] axis oriented parallel to the $a_{\xi'}$ axis of the underlying bulk.

We note that RHEED patterns were monitored from the surface prepared at different annealing temperatures up to 580 °C and also from the surface prepared under two different conditions described in Sec. III B. All of these preparation methods yield diffraction patterns with streak positions identical to that of the one presented in Fig. 2.

The chemical composition of the annealed surface is also determined. Annealing at about 550 °C yields the composition of $Al_{77}Pd_{20}Mn_3$, which is close to the bulk composition.

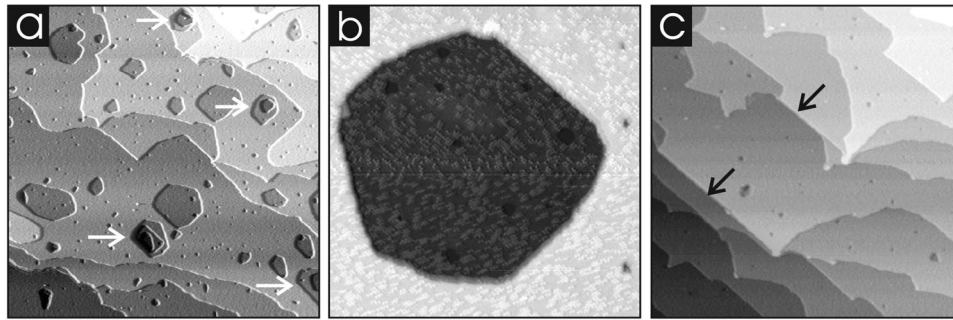FIG. 3. STM images of the pseudo-tenfold surface of the ξ'-Al$_{77.5}$Pd$_{19}$Mn$_{3.5}$ approximant for preparation I (see text) displaying (a) individual and hierarchal (shown by white arrows) pentagonal pits (area A: 1000 nm $\times$ 1000 nm), (b) a pentagonal pit in magnified scale (A: 150 nm $\times$ 150 nm), and (c) double steps, indicated by black arrows (A: 500 nm $\times$ 500 nm).

We also monitored the RHEED patterns during sputtering of the annealed surface. The streaked patterns disappear as soon as sputtering starts and the spotty patterns reappear only after 15 min sputtering with 3 keV Ar$^+$ for the given sample-ion gun geometry. Prior to each new annealing experiment, the surface was sputtered until the spotty patterns were obtained. We used a similar process to prepare the surface for STM studies presented in Sec. III B.

Finally, we present a possible explanation of why the sputter-induced layer prefers to have a single-domain structure rather than multiply twinned domains. As discussed above, the sputter-induced layer has a cubic structure with a $(1\bar{1}0)$-type surface plane and a lattice constant a close to that of CsCl-type Al–Pd. The [001] and [110] axes of the $(1\bar{1}0)$-type plane are oriented along the $\mathbf{c}_{\xi'}$ and $\mathbf{a}_{\xi'}$ axes of the bulk. The lattice parameters along these axes are a and $a\sqrt{2}$, which are close to $c_{\xi'}/4$ and $a_{\xi'}/6$, respectively. Along the $\mathbf{a}_{\xi'}$ axis, the lattice mismatch is about 7% with respect to the lattice constant of Al–Pd, while the respective value along the $\mathbf{c}_{\xi'}$ axis is about 3%. Because of this relatively small lattice mismatch, epitaxial film of Al–Pd alloy can be formed commensurately and it is likely that the layer develops in a single domain instead of multiply twinned domains.

B. Scanning tunneling microscopy

In this section, STM results from the surface obtained under two different preparation conditions are discussed. For the first preparation (preparation I), the sample was mechanically polished and degassed at 465 °C for 15 h. Subsequently, 14 sputter-annealing cycles were performed. Maximum annealing temperature was 580 °C (total annealing time was about 18 h). STM images of the thus obtained surface are shown in Figs. 3(a)–3(c). These images reveal a predominant step height of about 0.8 nm. In addition, steps of 1.6 nm height are observed occasionally [indicated by black arrows in in Fig. 3(c)]. The step height of 0.80 nm corresponds to one-half of the lattice constant along the $\mathbf{b}_{\xi'}$ axis in agreement with previously reported results.[41,42]

Terraces are very large (up to several hundred nanometers wide) and contain pits of different sizes (a few nm to hundreds of nm in diameter) and of mostly a uniform depth equal to a single-step height (0.80 nm). Many of these pits have a pentagonal shape with their edges oriented parallel to step edges of terraces. In some places, pits are arranged hierarchically. More interestingly, the pentagonal pits have the same orientation in a single terrace, but are rotated by 36° with respect to those in the adjacent terraces. This reflects the inversion symmetry relating the bulk layers located at 0.80 nm separation.

After the first set of measurements, the sample was taken out of the UHV chamber and subjected to a different preparation (preparation II). The sample was repolished, degassed at 420 °C for 4 h, and then three sputter-annealing cycles were carried out. In the first and second cycles, the sample was annealed at 510 °C followed by a 580 °C flash. In the last cycle, the sample was only flash annealed to about 580 °C. The total annealing time was about 3 h, which is much shorter than in preparation I. STM images of the resulting surface show fairly large terraces with almost no pits [Figs. 4(a)–4(d)]. Occasional screw dislocations were found on the surface. One example is given in Fig. 4(d). A screw dislocation has also been observed in a specific quasicrystalline system: namely, i-Al–Cu–Fe.[23]

In contrast to the predominant step height of 0.80 nm observed for preparation I, preparation II yields additional steps of smaller height [Fig. 4(c)]. The observed step heights are 0.80 nm and in addition the newly measured 0.40 ($\pm$0.05) nm. A line profile across the terraces of image 4(c) illustrates these two different step heights [Fig. 4(e)]. The 0.80-nm-high steps are observed most frequently on the surface, while only a few parts of the surface exhibit the steps of height close to 0.40 nm. The nonhomogeneous distribution of step heights on the surface may be due to a temperature gradient at the surface caused by the heating mechanism. As the annealing time during surface preparation was short, some parts of the surface may not have reached fully equilibrium states to obtain the usual surface termination and hence yield unusual step heights.

The layer's position in the unit cell of the bulk structure model of the ξ'-Al–Pd–Mn phase is illustrated in Fig. 4(f) (we denote different layers by A, B, C, and D for simplicity). Layers A, B, and D have almost same atomic density (number of atoms per layer), while the respective value of layer C is only about a half. The usual surface termination consists of incomplete D-type layers atop of B- and C-type layers. The white-dot-like features (which have a uniform height of
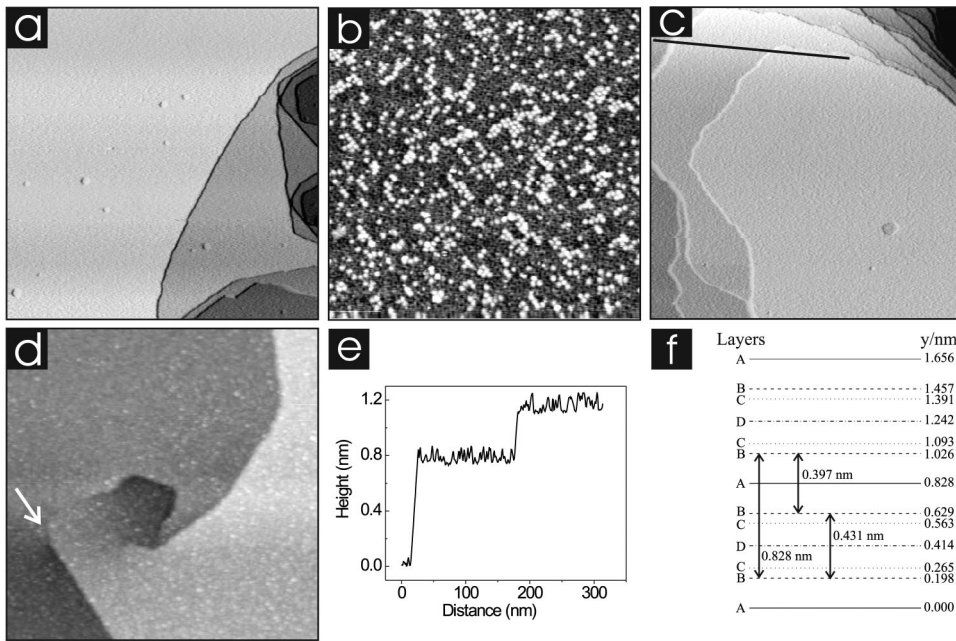
FIG. 4. STM images of the pseudo-tenfold ξ'-Al$_{77.5}$Pd$_{19}$Mn$_{3.5}$ surface for preparation II (see text) showing (a) large terraces with almost no pits (A: 700 nm × 700 nm), (b) high-resolution image on a terrace (A: 75 nm × 75 nm), (c) steps of different heights (A: 500 nm × 500 nm), and (d) screw dislocation (A: 200 nm × 200 nm), pointed by an arrow. (e) Line profile across terraces of image c. (f) A schematic diagram of layer positions in the unit cell of the bulk structure of ξ'−Al−Pd−Mn phase (Ref. 40). Equivalent layers are represented by identical style lines.

0.20 nm) observed in the high-resolution image [Fig. 4(b)] represent the incomplete D-type layer, while the darker region originates from B- and C-type layers below (see Ref. 41 for a detailed description). The step height of 0.80 nm (bottom to bottom distance of the adjacent terraces) corresponds to the separation of B-type layers located at $y=0.198$ nm and 1.026 nm.

The smaller step heights of about 0.40 nm (again, bottom to bottom distance of the adjacent terraces) also match the layer separation of the bulk model. Closely matching values are distance between consecutive B layers (i.e., 0.397 nm and 0.431 nm) and the separation of B layers at $y=1.026$ nm and 0.198 nm from the layer C at $y=0.563$ nm (i.e., 0.365 nm and 0.463 nm). This suggests that the possible origin of the newly observed terraces is either layer B at $y=0.629$ nm or layer C at $y=0.563$ nm. It is most likely that both B- and C-type layers are imaged by STM because these layers are so close that the tip could probe both.

The corrugation of all observed terraces is roughly equal [see line scan in Fig. 4(e)]. The height difference between maxima and minima of the line profile across terraces is roughly 0.20 nm. The value 0.20 nm is close to the separation of layer B at $y=0.629$ nm and layer A at $y=0.828$ nm, suggesting that the newly observed terraces consist of incomplete A- type layer atop of B- and C-type layers. The previous observations of a single-step height[41,42] and the present finding of different step heights share a common feature. In both cases, terraces form on B- and C-type layers. Assuming that these two types of layers constitute a single puckered layer, the atomic density of this puckered layer would be higher than that of any other single layer and terraces may have been preferably formed on this high-atomic-density layer.

In the following, we discuss the origin of the pits on terraces. As described above, the surface obtained under preparation I exhibits a high density of pits. However, these pits

almost do not appear on the surface obtained under preparation II. In both types of preparation, the maximum annealing temperature was the same (580 °C), the main difference being the annealing time which was much longer in preparation I. These results can be understood in terms of the bulk vacancy aggregation model proposed by different groups for i-Al−Pd−Mn quasicrystal.[39,46,47] It has been shown that both quasicrystal and approximant phases contain a significant amount of bulk vacancies.[39,48] The precise vacancy concentration in a specific sample critically depends on its thermal history, either during the growth process itself or during subsequent annealing treatments. This concentration has been estimated to be of the order of 1 at. % in as-grown Al−Pd−Mn quasicrystalline samples.[39,46] Upon annealing at sufficiently high temperature, individual atomic vacancies migrate toward the surface and condense to form voids affecting the surface morphology.[39,46] The formation of voids has been observed so far by mainly scanning electron microscopy[39,46,49–51] or optical microscopy.[46] With the lateral resolution of these techniques, the typical size of the voids is of the order of $1−10$ μm.[39,46,49–51] Much larger voids (>100 μm) have been observed in long-term preannealed i-Al−Pd−Mn samples (>1000 h at 800 °C).[51] The voids can further grow by Ostwald ripening.[52] The vacancy aggregation in voids reduces the vacancy concentration in the remaining material around the voids, leaving μm-sized smooth regions surrounding the voids.[46,50,51] The formation of the voids has been described as a negative growth, in analogy to epitaxial growth.[46] The diffusion of vacancies from the bulk toward the surface is equivalent to the adsorption of atoms from the vapor phase at the surface. Then nucleation occurs via surface diffusion and aggregation of vacancies.

The fact that the nm-sized pits are observed by STM for specific annealing treatment suggests that pit formation is a thermally activated process, like the formation of μm-sized voids. We hypothesize that the relatively long annealing process used in preparation I allowed the diffusion and conden-

sation of a significant amount of individual vacancies at the surface. The vacancy diffusion within the surface plane is considered to be a relatively easy process[46] and thus these individual vacancies can form pits by surface diffusion and aggregation. This is equivalent to a nucleation and growth process in the negative-growth model mentioned above. The fact that no pits are formed under preparation II could mean that the annealing was too short to allow the diffusion and condensation of a sufficient concentration of vacancies necessary to form observable pits at the surface. It could also mean that the annealing treatment used in preparation I led to the formation of a thick vacancy-depleted region below the surface. Schmithüsen estimated that the thickness of this depleted zone could be as large as several microns for an i-Al−Pd−Mn sample heat treated at 600 °C for 30 h.[46] It is then conceivable that the weak polishing used between preparations I and II (subsequent diamond paste of 6, 3, 1, and 0.25 μm, 3 min each) leads to a sample terminated by the vacancy-depleted zone. In such a case, no vacancy could segregate toward the surface, explaining the absence of pits under preparation II.

Here, we compare the nature of the presently detected pits with that of voids previously observed in i-Al−Pd−Mn by different groups.[39,46,47,49−51,53,54] By employing STM, we were able to detect the pits in nm scale. The length scale of the pits is thus different than that of the μm-sized voids identified by optical microscopy,[46] scanning electron microscopy,[39,46,49−51] and also atomic force microscopy.[53,54] The smaller size of the pits observed by STM could result from the aggregation of only surface or near-surface atomic vacancies. In other words, the nm-sized pits observed by STM constitute the first stage of the growth process that would lead upon a longer annealing time to the formation of the larger pits with μm size by coalescence or coarsening. Also, we should mention that due to the small lateral scale probed by the STM (usually <1 μm), we are blind with respect to supmicron morphology. Therefore, we cannot exclude that after preparation II, μm-sized pits exist at the surface, and we are scanning on a flat macroscopic region within or away from the pits. We note also that the pits are faceted, adopting the fivefold symmetry of the substrate. Similar faceting of the μm-sized voids is believed to be related to elastic strain relaxation.[46] Finally, we note that the depth of the pits is a multiple of the step height ($\sim b/2$), which corresponds to expectations in the negative-growth model, because islands formed in simple homoepitaxy experiment have an height that corresponds to the step height and they furthermore adopt a geometrical shape that match the substrate symmetry [for example, square islands of a single-step height are observed in Ag/Ag(100) homoepitaxy].[55]

The smaller lateral size and shallow depth of the pits as well as the fact that the pits are observed only on the surface prepared using longer annealing may also suggest evaporation as another possible process that leads to the formation of the pits. Excess annealing may have caused the evaporation of atoms from selective parts of the terraces. There are, however, two arguments that tend to disregard this possibility. First, it is known for ordinary crystals that evaporation primarily takes place at step edges or kink sites, because atoms

here are more weakly bound than when embedded in the middle of a flat terrace. However, it is not so clear that the same holds true for quasicrystals or approximants, for which the bonding energetic is much more complex than in simple metal systems. In both quasicrystals and approximants, a network of clusters glued by individual atoms can be recognized in their atomic structure and the bonding energetic may be different for glue atoms and cluster atoms, regardless of their location. For example, there is some experimental evidence showing that the cluster sites are more energetically favorable than the glue sites for the ξ'-Al−Pd−Mn approximant.[41] Therefore, one cannot rule out completely the possibility of evaporation based on this sole argument, as step edges or kink sites may still have higher bonding energy than that some terrace sites. The second argument against evaporation is the surface chemical composition measured by XPS after preparation I which is very close to the bulk composition. This rules out a substantial evaporation during annealing. This result also agrees with a detailed analysis of the evaporation in i-Al−Pd−Mn by Schmithüsen *et al.*, showing that the onset of evaporation occurs at about 630 °C in this system.[56] They also mentioned that evaporation appeared to be simply controlled by the vapor pressure of the elements with no influence of the quasicrystalline structure, and therefore this should hold true for the ξ'-Al−Pd−Mn approximant. We note, however, that it is very hard to detect experimentally the very small amount of material involved in the formation of evaporation pits. In conclusion, although evaporation as another process for pit formation cannot be ruled out completely, we believe that the vacancy aggregation model is more prone to explain the formation of pits observed on the surface of the ξ'-Al−Pd−Mn approximant.

IV. CONCLUSIONS

We have investigated the pseudo-tenfold surface of the ξ'-Al$_{77.5}$Pd$_{19}$Mn$_{3.5}$ crystal, an approximant of icosahedral Al−Pd−Mn quasicrystal, by employing RHEED and STM. The presented RHEED data constitute the first results on an approximant surface. Information on structural transitions in the surface region induced by sputtering and annealing is achieved by RHEED. The RHEED patterns of the surface after sputtering are found to be spotty, suggesting significant roughness in the surface region. These patterns can be explained by diffraction from a simple cubic lattice with $(1\bar{1}0)$-type surface plane and a lattice constant (a) close to that of the CsCl-type Al−Pd alloy. The [001] and [110] axes of the $(1\bar{1}0)$ surface plane are oriented parallel to the $\mathbf{c}_{\xi'}$ and $\mathbf{a}_{\xi'}$ axes of the bulk, respectively. The lattice parameters of the cubic lattice are closely related to those of the bulk by $c_{\xi'} \approx 4a$ and $a_{\xi'} \approx 6\sqrt{2}a$, respectively. As a result of this relationship, the sputter-induced layer can be accommodated on the underlying substrate with only a small strain. In this scenario, the layer develops in a single domain instead of multiply twinned domains observed on sputtered quasicrystal surfaces, where five (or ten) domains are observed at every 72° (or 36°) rotation around the surface normal.

XPS from the sputtered surface reveals a depletion of Al in the surface region. Annealing the sputtered surface, how-

ever, restores the chemical composition of the bulk. RHEED patterns of the annealed surface are rather streaky with strong diffraction spots aligned on circles revealing a very flat surface. In these patterns, the diffraction streaks yield a periodic spacing. The corresponding real space value of the streaks separation is found to be consistent with the bulk lattice constant.

STM of the sputter-annealed surface reveals flat terraces in agreement with the previous RHEED observations. The surface prepared under different preparation methods is found to exhibit different step-height distribution and terrace morphology. A longer annealing yields a high density of pits on the terraces. The orientation of these pits as well as step edges reflects the in-plane fivefold symmetry. We have provided arguments suggesting that the formation of the faceted pits is more likely due to bulk vacancy diffusion at surfaces upon long annealing rather than evaporation. The aggregation of the vacancies into faceted pits could be promoted by easy in-plane vacancy diffusion. The terraces are separated predominantly by 0.80-nm-high steps and occasionally by double steps. In contrast to these observations, the surface prepared with shorter annealing time exhibits highly perfect terraces with 0.80-nm-high steps and additional unusual steps of heights close to 0.40 nm. All step heights observed for both preparation methods are consistent with interlayer spacings of the bulk model.

Finally, we come back to the question raised in the Introduction about similarities and differences among surface phenomena in quasicrystals and approximants. We found that most features observed for the investigated approximant surface closely resemble characteristics found for quasicrystal surfaces. These include different surface terminations upon different surface treatments, the development of different step-height distributions and terrace morphologies under different preparation methods, and the characteristic of bulk truncation found for sputter-annealed surfaces. A clear difference is observed for the sputtered surface. The sputtered approximant surface yields crystalline layers of a single domain in the surface region in contrast to a multiply twinned domain structure found in quasicrystal surfaces. We argued that the crystal structure of the underlying bulk is responsible for the development of the single-domain structure.

ACKNOWLEDGMENTS

*Corresponding author. Electronic address: hemraj.sharma@nims.go.jp

[1] A. P. Tsai, in *Physical Properties of Quasicrystals*, edited by Z. M. Stadnik (Springer, Berlin, 1999).

[2] A. I. Goldman and R. F. Kelton, Rev. Mod. Phys. **65**, 213 (1993).

[3] Z. M. Stadnik, in *Physical Properties of Quasicrystals*, edited by Z. M. Stadnik (Springer, Berlin, 1999).

[4] P. A. Thiel, A. I. Goldman, and C. J. Jenks, in *Physical Properties of Quasicrystals*, edited by Z. M. Stadnik (Springer, Berlin, 1999).

[5] T. M. Schaub, D. E. Bürgler, H.-J. Güntherodt, and J. B. Suck, Phys. Rev. Lett. **73**, 1255 (1994).

[6] M. Gierer, M. A. Van Hove, A. I. Goldman, Z. Shen, S.-L. Chang, C. J. Jenks, C.-M. Zhang, and P. A. Thiel, Phys. Rev. Lett. **78**, 467 (1997).

[7] M. Gierer, M. A. Van Hove, A. I. Goldman, Z. Shen, S.-L. Chang, P. J. Pinhero, C. J. Jenks, J. W. Anderegg, C.-M. Zhang, and P. A. Thiel, Phys. Rev. B **57**, 7628 (1998).

[8] Z. Shen, M. J. Kramer, C. J. Jenks, A. I. Goldman, T. Lograsso, D. Delaney, M. Heinzig, W. Raberg, and P. A. Thiel, Phys. Rev. B **58**, 9961 (1998).

[9] D. Naumović, P. Aebi, C. Beeli, and L. Schlapbach, Surf. Sci. **433–435**, 302 (1999).

[10] Z. Shen, C. R. Stoldt, C. J. Jenks, T. A. Lograsso, and P. A. Thiel, Phys. Rev. B **60**, 14688 (1999).

[11] J. Ledieu, A. W. Munz, T. M. Parker, R. McGrath, R. D. Diehl, D. W. Delaney, and T. A. Lograsso, Surf. Sci. **433**, 666 (1999).

[12] D. Naumović, P. Aebi, L. Schlapbach, C. Beeli, T. A. Lograsso, and D. W. Delaney, Quasicryst. Proc. Int. Conf. **6**, 749 (1998).

[13] D. Naumović, P. Aebi, L. Schlapbach, C. Beeli, T. A. Lograsso, and D. W. Delaney, Phys. Rev. B **60**, R16330 (1999).

[14] D. Naumović, P. Aebi, L. Schlapbach, and C. Beeli, Mater. Sci. Eng., A **294–296**, 882 (2000).

[15] D. Naumović, P. Aebi, L. Schlapbach, C. Beeli, K. Kunze, T. A. Lograsso, and D. W. Delaney, Phys. Rev. Lett. **87**, 195506 (2001).

[16] B. Bolliger, M. Erbudak, A. Hensch, and D. D. Vvedensky, Mater. Sci. Eng., A **294–296**, 859 (2000).

[17] L. Barbier, D. Le Floćh, Y. Calvayrac, and D. Gratias, Phys. Rev. Lett. **88**, 085506 (2002).

[18] Z. Papadopolos, G. Kasner, J. Ledieu, E. J. Cox, N. V. Richardson, Q. Chen, R. D. Diehl, T. A. Lograsso, A. R. Ross, and R. McGrath, Phys. Rev. B **66**, 184207 (2002).

[19] J.-C. Zheng *et al.*, Phys. Rev. B **69**, 134107 (2004).

[20] R. S. Becker, A. R. Kortan, F. A. Thiel, and H. S. Chen, J. Vac. Sci. Technol. B **9**, 867 (1991).

[21] Z. Shen, P. J. Pinhero, T. A. Lograsso, D. W. Delaney, C. J. Jenks, and P. A. Thiel, Surf. Sci. **385**, L923 (1997).

[22] F. Shi, Z. Shen, D. W. Delaney, A. I. Goldman, C. J. Jenks, M. J. Kramer, T. A. Lograsso, P. A. Thiel, and M. A. V. Hove, Surf. Sci. **411**, 86 (1998).

[23] T. Cai *et al.*, Surf. Sci. **495**, 19 (2001).

[24] T. Cai, V. Fournée, T. Lograsso, A. R. Ross, and P. A. Thiel, Phys. Rev. B **65**, 140202(R) (2002).

[25] J. A. Barrow, V. Fournée, A. R. Ross, P. A. Thiel, M. Shimoda, and A. P. Tsai, Surf. Sci. **539**, 54 (2003).

[26] H. R. Sharma, V. Fournée, M. Shimoda, A. R. Ross, T. A. Lograsso, A. P. Tsai, and A. Yamamoto, Phys. Rev. Lett. **93**, 165502 (2004).

[27] E. G. McRae, R. A. Malic, T. H. Lalonde, F. A. Thiel, H. S. Chen, and A. R. Kortan, Phys. Rev. Lett. **65**, 883 (1990).

[28] A. R. Kortan, R. S. Becker, F. A. Thiel, and H. S. Chen, Phys. Rev. Lett. **64**, 200 (1990).

[29] M. Zurkirch, B. Bollinger, M. Erbudak, and A. R. Kortan, Phys. Rev. B **58**, 14113 (1998).

[30] M. Gierer, A. Mikkelsen, M. Gräber, P. Gille, and W. Moritz, Surf. Sci. **463**, L654 (2000).

[31] M. Shimoda, J. Q. Guo, T. J. Sato, and A. P. Tsai, Surf. Sci. **454–456**, 11 (2000).

[32] M. Kishida, Y. Kamimura, R. Tamura, K. Edagawa, S. Takeuchi, T. Sato, Y. Yokoyama, J. Q. Guo, and A. P. Tsai, Phys. Rev. B **65**, 094208 (2002).

[33] R. McGrath, J. Ledieu, E. J. Cox, and R. D. Diehl, J. Phys.: Condens. Matter **14**, R119 (2002).

[34] H. R. Sharma, W. Theis, P. Gille, and K. H. Rieder, Surf. Sci. **511**, 387 (2002).

[35] H. R. Sharma, K. J. Franke, W. Theis, A. Riemann, S. Fölsch, P. Gille, and K. H. Rieder, Surf. Sci. **561**, 121 (2004).

[36] N. Ferralis, K. Pussi, E. J. Cox, M. Gierer, J. Ledieu, I. R. Fisher, C. J. Jenks, M. Lindroos, R. McGrath, and R. D. Diehl, Phys. Rev. B **69**, 153404 (2004).

[37] J. Yuhara, J. Klikovits, M. Schmid, P. Varga, Y. Yokoyama, T. Shishido, and K. Soda, Phys. Rev. B **70**, 024203 (2004).

[38] H. R. Sharma, K. J. Franke, W. Theis, A. Riemann, S. Fölsch, P. Gille, and K. H. Rieder, Phys. Rev. B **70**, 235409 (2004).

[39] P. Ebert, M. Yurechko, F. Kluge, T. Cai, B. Grushko, P. A. Thiel,

and K. Urban, Phys. Rev. B **67**, 024208 (2003).

[40] M. Boudard, H. Klein, M. de Boissieu, and M. Audier, Philos. Mag. A **74**, 939 (1996).

[41] V. Fournée, A. R. Ross, T. A. Lograsso, J. W. Anderegg, C. Dong, M. Kramer, I. R. Fisher, P. C. Canfield, and P. A. Thiel, Phys. Rev. B **66**, 165423 (2002).

[42] V. Fournée, J. A. Barrow, M. Shimoda, A. R. Ross, T. A. Lograsso, P. A. Thiel, and A. P. Tsai, Surf. Sci. **147**, 541 (2003).

[43] M. Audier, M. Durand-Charre, and M. D. Boissieu, Philos. Mag. B **68**, 607 (1993).

[44] M. Hansen, *Constitution of Binary Alloys* (McGraw-Hill, New York, 1958).

[45] M. Shimoda, T. J. Sato, A. P. Tsai, and J. Q. Guo, Phys. Rev. B **62**, 11288 (2000).

[46] F. Schmithüsen, Ph.D. thesis, Université Grenoble, France, 2001.

[47] S. Agliozzo, J. Gastaldi, H. Klein, J. Härtwig, J. Baruchel, and E. Brunello, Phys. Rev. B **69**, 144204 (2004).

[48] F. Baier and H.-E. Schaefer, Phys. Rev. B **66**, 064208 (2002).

[49] P. Ebert, F. Yue, and K. Urban, Phys. Rev. B **57**, 2821 (1998).

[50] F. Kluge, P. Ebert, B. Grushko, and K. Urban, Mater. Sci. Eng., A **294–296**, 874 (2000).

[51] F. Kluge, M. Yurechko, K. Urban, and P. Ebert, Surf. Sci. **519**, 33 (2002).

[52] C. Beeli, T. Godecke, and R. Luck, Philos. Mag. Lett. **78**, 339 (1998).

[53] G. Cappello *et al.*, Mater. Sci. Eng., A **294–296**, 822 (2000).

[54] G. Cappello *et al.*, Phys. Rev. B **65**, 245405 (2002).

[55] P. A. Thiel and J. W. Evans, J. Phys. Chem. B **104**, 1663 (2000).

[56] F. Schmithüsen, G. Cappello, M. de Boissieu, M. Boudard, F. Comin, and J. Chevrier, Surf. Sci. **444**, 113 (2000).